

GMRT mini-survey to search for 21-cm absorption in Quasar-Galaxy Pairs at $z \sim 0.1$

N. Gupta^{1*}, R. Srianand², D.V. Bowen³, D.G. York⁴ and Y. Wadadekar⁵

¹ *Australia Telescope National Facility, CSIRO, Epping, NSW 1710, Australia*

² *Inter University Centre for Astronomy and Astrophysics, Post Bag 4, Ganeshkhind, Pune 411 007, India*

³ *Department of Astrophysical Sciences, Peyton Hall, Princeton University, Princeton NJ 08544, USA*

⁴ *Department of Astronomy & Astrophysics and Enrico Fermi Institute, 5640 S. Ellis Avenue, Univ. of Chicago, Chicago, IL 60637, USA*

⁵ *National Centre for Radio Astrophysics, Post Bag 3, Ganeshkhind, Pune 411 007, India*

Accepted. Received; in original form

ABSTRACT

We present the results from our 21-cm absorption survey of a sample of 5 quasar-galaxy pairs (QGPs), with the redshift of the galaxies in the range $0.03 \leq z_g \leq 0.18$, selected from the Sloan Digital Sky Survey (SDSS). The H I 21-cm absorption was searched towards the 9 sight lines with impact parameters ranging from ~ 10 to ~ 55 kpc using Giant Metrewave Radio Telescope (GMRT). 21-cm absorption was detected only in one case i.e. towards the Quasar ($z_q = 2.625$ SDSS J124157.54+633241.6) – galaxy ($z_g = 0.143$ SDSS J124157.26+633237.6) pair with the impact parameter ~ 11 kpc. The quasar sight line in this case pierces through the stellar disk of a galaxy having near solar metallicity (i.e. $(O/H)+12 = 8.7$) and star formation rate uncorrected for dust attenuation of $0.1 M_\odot \text{ yr}^{-1}$. The quasar spectrum reddened by the foreground galaxy is well fitted with the Milky Way extinction curve (with an A_V of 0.44) and the estimated H I column density is similar to the value obtained from 21-cm absorption assuming spin temperature (T_S) of 100 K.

In the remaining cases, our GMRT spectra provide upper limit on $N(\text{H I})$ in the range, $(10^{17} - 10^{18}) \times T_S \text{ cm}^{-2}$. Combining our sample with the $z \leq 0.1$ data available in the literature, we find the detectability of 21-cm absorption with integrated optical depth greater than 0.1 km s^{-1} to be 50% for the impact parameter less than 20 kpc. Using the surface brightness profiles and well established relationship between the optical size and extent of the H I disk known for *nearby* galaxies, we conclude that in most of the cases of 21-cm absorption non-detection, the sight lines may not be passing through the H I gas (1σ column density of few times 10^{19} cm^{-2}). We also find that in comparison to the absorption systems associated with these QGPs, $z < 1$ DLAs with 21-cm absorption detections have lower Ca II equivalent widths despite having higher 21-cm optical depths and smaller impact parameters. This suggests that the current sample of DLAs may be a biased population that avoids sight lines through dusty star-forming galaxies. A systematic survey of QGPs over a wider redshift range using a large sample is needed to confirm these findings and understand the nature of 21-cm absorbers.

Key words: quasars: active – quasars: absorption lines –

1 INTRODUCTION

Observations of galaxies via 21-cm line, both emission and absorption, have proven to be valuable for our understanding of the abundance and distribution of H I gas, and processes leading to star formation. In the local Universe, blind 21-cm

emission-line surveys using single-dish telescopes provide reliable measurements of the H I mass density (Zwaan et al. 2005). These surveys are complemented with the spatially resolved H I images obtained using interferometers to trace the large scale dynamics of the galaxies (e.g. Bosma 1981; Fisher & Tully 1981; Meyer et al. 2004; Oosterloo, Fraternali & Sancisi 2007; de Blok et al. 2008; Walter et al. 2008). Since H I gas in galaxies extends farther than the stellar disk, it

* E-mail: Neeraj.Gupta@csiro.au

is also the component of the galaxy that is most affected by interactions and is therefore a good tracer of tidal interactions and merger effects (Haynes, Giovanelli & Robert 1979; Rosenberg & Schneider 2002). However, beyond the local Universe (i.e. $z \gtrsim 0.2$) 21-cm emission is not easily detectable with current radio telescopes (Verheijen et al. 2007; Catinella et al. 2008). Therefore, H I 21-cm emission line observations need to be complemented with absorption line studies to trace the evolution of the atomic gas component of galaxies.

Unlike 21-cm emission, detectability of 21-cm absorption is not limited by distance and depends only on the strength of the background radio sources and 21-cm absorption cross-section of the galaxies. Due to the limitations imposed by the narrow receiver bandwidths and the hostile radio-frequency interference (RFI) environment, systematic blind searches of 21-cm absorption have not been possible till now. Consequently, a host of absorption-line surveys have been designed to detect 21-cm absorption from the gas pre-selected by the presence of a damped Lyman- α absorber (DLA) or Mg II absorption with a view to trace physical conditions in the interstellar medium of galaxies at $0 < z \leq 3.5$ (e.g. Briggs & Wolfe, 1983; Carilli et al. 1996; Lane 2000; Kanekar & Chengalur 2003, 2009a; Curran et al. 2007; Gupta et al. 2007, 2009; Srianand et al. 2010).

Although remarkable progress has been achieved in these emission and absorption line studies, an important missing link is the lack of understanding of the nature of absorption line galaxies required to establish a direct connection with the nearby galaxies detected in H I 21-cm emission. At $z \lesssim 2$, the most successful search for 21-cm absorbers, to date, has resulted from the Giant Metrewave Radio Telescope (GMRT) survey based on the sample of *strong* Mg II absorbers (rest equivalent width, $W_r(\text{Mg II } \lambda 2796) \geq 1.0 \text{ \AA}$) selected from the Sloan Digital Sky Survey (SDSS) database (Gupta et al. 2009). Connections between Mg II absorbers and galaxies at these redshifts are established by either searching for the galaxy responsible for the Mg II absorption in QSO spectra or by searching for Mg II absorption lines at the redshifts of known galaxies in the spectra of background QSOs. Based on the first approach, it is found that the success rate of detecting L_* galaxies at the same redshift as the known strong Mg II absorbers is close to unity (e.g. Bergeron & Boissé 1991; Steidel 1995). The second approach shows that galaxies close to QSO sight lines do not always produce detectable absorption (see Bechtold & Ellingson 1992; Tripp & Bowen 2005). The existing observations are consistent with Mg II absorption originating from extended gas halos with covering factors much less than unity (see Churchill et al. 2005; Kacprzak et al. 2008). The presence of large number of high quality QSO spectra in the SDSS database allows (i) the direct detection of emission lines from these galaxies superimposed on the QSO spectra (Quashnock et al. 2008; Noterdaeme, Srianand & Mohan 2010; Borthakur et al. 2010) and (ii) detection of emission lines in the stacked spectra (Noterdaeme et al. 2010; Ménard et al. 2009). These observations are consistent with strong Mg II systems being produced by gas within ~ 10 kpc of a star-forming galaxy.

The 21-cm optical depth, in addition to H I column density, $N(\text{H I})$, also depends on the spin temperature (T_s). As, to begin with, there is no direct relationship between

$W_r(\text{Mg II})$ and $N(\text{H I})$ it is difficult to use the results of Mg II systems alone to establish the connection between 21-cm absorbers and galaxies. A systematic survey of 21-cm absorption in a sample of bright radio sources with sight lines passing through the gas disks/halos of foreground galaxies is required to determine the 21-cm absorption cross-section of the galaxies. The availability of large number of spectra in the SDSS database allows us to build a complete sample of associations of radio sources and galaxies suitable for this purpose. We refer to these fortuitous associations as quasar-galaxy pair (QGP) if the background radio source is a quasar, and radio source-galaxy pair (RGP) if the background source is a radio galaxy. As a prelude to our systematic survey to search for 21-cm absorption in a complete sample of QGPs and RGPs (foreground galaxy redshift $z_g \lesssim 0.3$) selected from SDSS database, we have searched for 21-cm absorption in 5 QGPs as a pilot project with GMRT. The purpose of this paper is to present the results from the observations of these 5 QGPs. In Section 2, we present the details of GMRT observations and data analysis. The details of QGPs, their radio and optical properties, and results from the GMRT observations are presented in Section 3. In Section 4, we discuss the detectability of 21-cm absorption by combining our sample with the data from the literature. Results are summarised in Section 5. Throughout this paper we use the Λ CDM cosmology with $H_0 = 71 \text{ km s}^{-1} \text{ Mpc}^{-1}$, $\Omega_m = 0.27$ and $\Omega_\Lambda = 0.73$ (Spergel et al. 2007).

2 OBSERVATIONS AND DATA REDUCTION

Our sample of 5 QGPs presented in Table 1 is drawn from the SDSS DR5 database. The sample was constructed by cross-correlating SDSS DR5 photometric and spectroscopic database for QSOs and galaxies with the FIRST and NVSS surveys to identify QGPs with background quasar flux density at 1.4 GHz in excess of ~ 50 mJy. Redshifts for the galaxies for 4 QGPs presented here were obtained from the publicly available SDSS spectra. For the remaining quasar ($z_q = 2.130$ SDSS J082153.82+503120.4) – galaxy ($z_g = 0.184$ SDSS J082153.75+503125.7) pair, we have estimated the galaxy redshift using our own Apache Point Observatory (APO) 3.5-meter telescope observations. We also obtained the APO 3.5-meter telescope observations for quasar ($z_q = 0.584$ SDSS J084957.97+510829.0) – galaxy ($z_g = 0.073$ SDSS J084957.48+510842.3) pair to complement the SDSS spectrum. Optical parameters used in this study are extracted from the SDSS photometric and spectroscopic database and the data obtained from our APO observations. Details of these optical data are provided in the subsequent sections.

We observed our sample of 5 QGPs using the GMRT L-band receiver. For these observations we used the 2 MHz baseband bandwidth split into 128 frequency channels (spectral resolution $\sim 4 \text{ km s}^{-1}$ per channel) centered at the redshifted H I frequency estimated from galaxy redshifts. The observing log is presented in Table 1. Data were acquired in the two linear polarization channels called XX and YY. We observed the standard flux density calibrators 3C 48, 3C 147 and 3C 286 for 10-15 mins every 2-3 hrs to obtain reliable flux and bandpass calibration. A phase calibrator was also observed for 10 mins every ~ 45 mins. GMRT data were re-

Table 1. Observing log for the GMRT observations.

Quasar	z_q	r mag	Galaxy	z_g	Date	Channel width (km s^{-1})	Time (hrs)
(1)	(2)	(3)	(4)	(5)	(6)	(7)	(8)
J082153.82+503120.4	2.130	17.8	J082153.75+503125.7	0.1835	2007 Sep 19	3.9	8.0
J084957.97+510829.0	0.584	18.2	J084957.48+510842.3	0.0734	2007 Jun 19	3.5	7.7
J111023.85+032136.1	0.966	18.6	J111025.09+032138.8	0.0301	2008 Mar 01	3.4	7.6
J122847.42+370612.0	1.517	18.2	J122847.72+370606.9	0.1383	2008 Mar 02	3.7	7.5
J124157.54+633241.6	2.625	17.9	J124157.26+633237.6	0.1430	2008 Mar 03	3.8	7.7
					2009 Jun 13	3.8	8.0
					2009 Jun 14	3.8	5.4

Column 1: Quasar name. Column 2 and 3: Quasar redshift and r -band magnitude respectively. Column 4: Galaxy name. Column 5: Galaxy redshift. Column 6: Date of observation. Column 7: channel width in km s^{-1} . Column 8: time on source in hrs.

duced using the NRAO Astronomical Image Processing System (AIPS) following the standard procedures. After the initial flagging and calibration, source and calibrator data were examined to flag and exclude the baselines and timestamps affected by RFI. Applying complex gains and bandpass obtained using the flux and phase calibrators, a continuum map of the source was made using absorption-free channels. Using this map as a model, self-calibration complex gains were determined and applied to all the frequency channels. The same continuum map was then used to subtract the continuum emission from the dataset. This continuum subtracted dataset was then imaged separately for the channels XX and YY to get 3-dimensional (third axis being the frequency) data cubes. The spectra at the location of radio components of interest were extracted from these cubes and compared for consistency. If necessary a first-order cubic-spline was fitted to remove the residual continuum from the spectra. The two polarization channels were then combined to get the final stokes I spectrum, which was then shifted to the heliocentric frame.

3 RESULTS

This survey of 5 QGPs resulted in the detection of 21-cm absorption from one QGP whereas no 21-cm absorption was detected for the remaining four QGPs. Results are summarised in the Table 2. In the following, we present results for the individual QGPs.

3.1 Details of the QGP with 21-cm absorption detection

Quasar ($z_q = 2.625$ SDSS J124157.54+633241.6) – galaxy ($z_g = 0.143$ SDSS J124157.26+633237.6) pair: The background quasar J124157.54+633241.6 is only at a projected separation of $4.4''$ from the foreground galaxy at the redshift, $z_g = 0.143$. The quasar sight line is within the r -band Petrosian radius (R_{90}) that contains 90% of the Petrosian flux from galaxy (see Table 2). As can be seen from the Fig. 1, the quasar sight line pierces through the stellar disk of the foreground galaxy.

The galaxy redshift is measured using its emission lines superimposed on top of the QSO continuum in



Figure 1. Color representation of the quasar ($z_q = 2.625$ SDSS J124157.54+633241.6)–galaxy ($z_g = 0.143$ SDSS J124157.26+633237.6) pair. The image is $77''$ on a side, with north-east towards the top left corner, and centered on the QSO.

the SDSS fiber spectrum. $H\alpha$, $H\beta$, $[\text{S II}]\lambda\lambda 6718, 6732$ and $[\text{N II}]\lambda\lambda 6549, 6585$ are clearly detected. These emission lines were fitted with Gaussians using χ^2 minimization keeping the same redshift for all the lines (see Fig 2). The best fitted emission redshift is $z_{\text{em}} = 0.1430 \pm 0.0001$. The integrated emission line fluxes are summarized in Table 3. The measured ratio of different line fluxes with respect to that of $H\alpha$ in this system and from the SDSS template spectra of galaxies are also given in this table. Clearly the line ratios that are indicators of metallicity and reddening are consistent with average late type galaxies found in the SDSS.

The Balmer line ratio, $F(H\alpha)/F(H\beta)$, has large error mainly due to the fact that $H\beta$ is weak and present on top of the C IV emission line of the QSO. Following Argence & Lamareille (2009) we get the optical depth at the intrinsic V-band of the galaxy, $\tau_V^{\text{Balmer}} = 1.4_{-1.3}^{+2.0}$, using

Table 2. Results of GMRT observations and other parameters derived from the SDSS data.

Quasar	Peak flux (mJy)	Spectral rms (mJy/b/ch)	τ	$\int \tau dv$ (km s ⁻¹)	Petrosian Radius (R ₉₀) (")	Angular Separation (")	Impact parameter (kpc)	W _r (Ca IIλ3935) (Å)
(1)	(2)	(3)	(4)	(5)	(6)	(7)	(8)	(9)
J0821+5031	47.8	0.9	<0.019	<0.38	3.48	5.2	15.9	<0.25
J0849+5108	248	1.0	<0.004	<0.08	11.22	14.1	19.4	<2.40
J1110+0321C	7.6	1.0	<0.132	<2.80	11.74	18.8	11.2	<0.85
J1110+0321E	155	1.1	<0.007	<0.13	37.9	22.5	–
J1110+0321W	223	0.9	<0.004	<0.08	25.7	15.3	–
J1228+3706	298	1.1	<0.004	<0.07	3.38	6.2	15.0	0.49±0.13
J1241+6332C	67.9	0.7	0.157	2.90	4.42	4.4	11.0	1.01±0.11
J1241+6332E	6.21	0.7	<0.113	<2.50	13.6	34.0	–
J1241+6332W	22.9	0.7	<0.031	<0.62	21.2	53.0	–

Column 1: Radio component. Column 2: Peak flux density in mJy. Column 3: Spectral rms in mJy beam⁻¹ channel⁻¹. Column 4: Maximum of optical depth or 1σ limit to it. Column 5: Integrated 21-cm optical depth or 3σ upper limit in case of non-detections with data smoothed to 10 km s⁻¹. Column 6: Petrosian radius that contains 90% of the Petrosian flux from galaxy as measured using r-band SDSS images. Columns 7 and 8: Angular separation and the projected distance between the radio component (quasar) and centre of galaxy respectively. Column 9: Rest equivalent width of Ca IIλ3935 or 3σ upper limit to it.

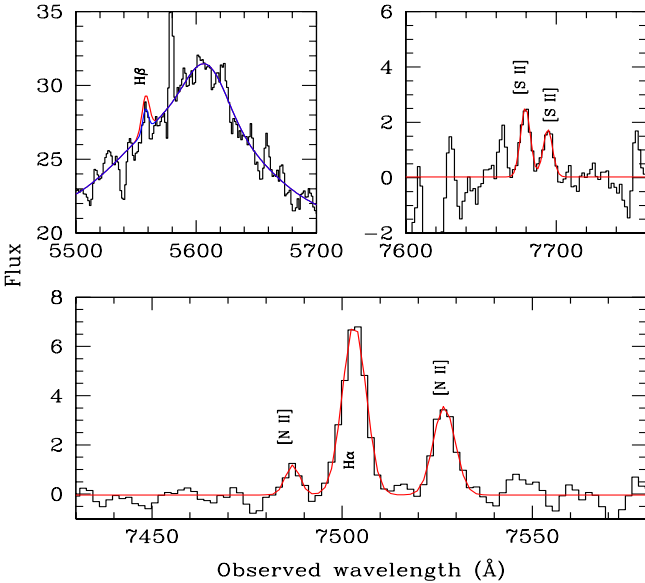


Figure 2. Gaussian fits to the emission lines detected from the galaxy SDSS J124157.26+633237.6. The Hβ line falls on the C IV emission line of the QSO. Double Gaussian fit to this broad emission line is also shown.

$$\tau_V^{\text{Balmer}} = \frac{\ln\left(\frac{H\beta}{H\alpha}\right) - \ln\left(\frac{H\beta^i}{H\alpha^i}\right)}{\frac{\tau_\beta}{\tau_V} - \frac{\tau_\alpha}{\tau_V}} \quad (1)$$

and the intrinsic Balmer ratio $H\beta^i/H\alpha^i = 2.85$ (Osterbrock & Ferland 2006) and τ_λ as given by the Eq. 3 of Wild et al. (2007a). Such high values are usually seen in high metallicity galaxies (see Fig. 1 of Argence & Lamareille 2009).

We get an independent estimate of τ_V and E(B-V) along the sight line to the QSO by fitting the QSO spectral energy distribution (SED) using the SDSS composite QSO spectra reddened by the Milky Way extinction curve and the method used in Srianand et al (2008) and Noterdaeme et al. (2009). The best fit (with $\chi_\nu^2 = 1.4$) to the observed spectrum (see

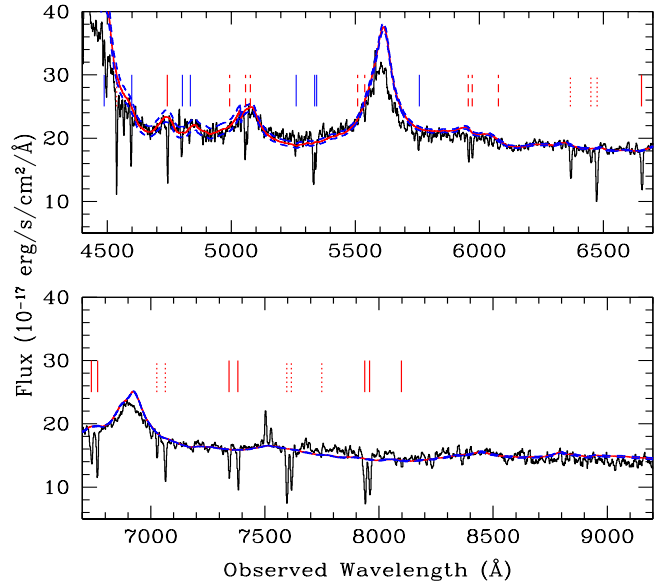


Figure 3. SDSS spectrum of the QSO SDSS J124157.54+633241.6. The spectral energy distribution from the SDSS composite spectrum reddened by the dust in the 21-cm absorbing galaxy is also over-plotted with the associated 1σ error. We also mark the locations of different absorption lines originating from other intervening Mg II and C IV absorbers along the line of sight. The doublet near 7950 Å corresponds to Mg IIλλ2796,2803 of an absorbing system at $z_{abs} = 1.840$ (solid red indicators). The doublets near 7600 Å and 5950 Å are Mg IIλλ2796,2803 from systems at $z_{abs} = 1.717$ (dashed red indicators) and $z_{abs} = 1.130$ (long dashed red indicators) respectively. The C IV absorber at $z_{abs} = 2.444$ is marked with solid blue indicators.

Fig. 3) is obtained for $A_V = 0.44 \pm 0.04$, where $A_\lambda = 1.086 \tau_\lambda$. Note that in principle the two measurements of τ_V (or A_V) need not agree with the one based on Balmer decrement as the properties of the absorbing gas along the QSO sight

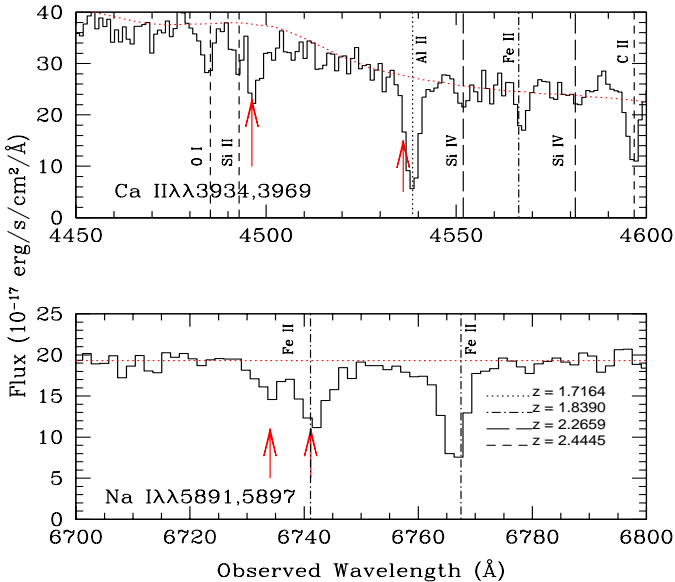


Figure 4. SDSS spectrum of the QSO SDSS J124157.54+633241.6. Arrows mark the expected locations of Ca II and Na I absorption from $z_g = 0.143$ galaxy. The vertical lines mark the metal absorption lines from other intervening systems.

line need not be identical to that of the emitting region covered by the fiber. If we use the relationship between A_V and $N(\text{H I})$ observed for the Milky Way we get

$$N(\text{H I}) = \left(\frac{1}{\kappa}\right) 7 \times 10^{20} \text{cm}^{-2}. \quad (2)$$

Here, κ is the ratio of dust-to-gas ratio in the absorption system to that in the Milky Way. Note that the extinction we find is higher than what is typically found along the QSO sight lines with Mg II and Ca II absorbers (York et al. 2006; Wild, Hewett & Pettini 2006) and less than that seen towards absorption systems with 2175 Å dust absorption (Srianand et al. 2008).

Next we estimate the total star formation rate (SFR) in the portion of the 21-cm absorbing galaxy that is covered by the SDSS fiber. For this we use (Argence & Lamareille 2009) ,

$$\log(SFR) = 0.95 * \log L(\text{H}\alpha) - \log \eta_{\text{H}\alpha}. \quad (3)$$

Adopting standard cosmological parameters, we get uncorrected luminosity of $L(\text{H}\alpha) = 3.0 \times 10^{40}$ erg/s. Using $\log(\eta_{\text{H}\alpha}) = 39.38$ (Argence & Lamareille 2009) we get SFR uncorrected for dust attenuation (and fiber filling factor) of $0.1 M_{\odot} \text{yr}^{-1}$. Using the integrated fluxes of H α and N [II] λ 6549 lines and the linear relationship given in Pettini & Pagel (2004) we get $12+\log(\text{O}/\text{H}) = 8.7$, suggesting super-Solar metallicity in the emission line region. This is slightly higher than the mean value measured by Argence & Lamareille (2009) for their whole sample. The inferred (O/H) and τ_V^{Balmer} values are consistent with those found for their high metallicity sub-sample. Interestingly, the inferred metallicity in this system is higher than the values obtained by Noterdaeme, Srianand & Mohan (2010) for the sample of [O III] emitting Mg II absorbers at $0.4 \leq z \leq 0.7$

Table 3. Emission line parameters of the galaxy SDSS J124157.26+633237.6

Line(l)	$F_{\lambda}(10^{-17} \text{erg s}^{-1} \text{cm}^{-2})$	$F(\text{H}\alpha)/F_l$	$F^c(\text{H}\alpha)/F_l^c$
H α	56.6 ± 4.3	1.0	1.0
H β	12.5 ± 5.5	$4.5^{+4.2}_{-1.6}$	2.8
[N II] λ 6549	10.0 ± 3.5	$5.7^{+3.7}_{-1.8}$	5.7
[N II] λ 6585	28.0 ± 4.3	$2.0^{+0.6}_{-0.4}$	2.0
[S II] λ 6718	12.9 ± 3.6	$4.4^{+2.1}_{-1.2}$	4.5
[S II] λ 6732	6.5 ± 3.6	$8.7^{+12.3}_{-3.5}$	8.9

F^c : Flux corrected for dust attenuation.

and consistent with that measured in a few strong Ca II absorbers (see Zych et al. 2007).

The SDSS spectrum of the quasar shows the Na I λ 5891 and Ca II λ 3934 absorption lines at the redshifted wavelengths expected for the foreground galaxy (see Fig. 4). The other members of the Na I and Ca II doublet are blended with the other intervening absorption lines. The rest equivalent widths of Ca II λ 3934 and Na I λ 5891 absorption lines are $1.01 \pm 0.11 \text{ \AA}$ and $0.85 \pm 0.10 \text{ \AA}$ respectively. The measured rest equivalent width of Ca II λ 3934 is much higher than that measured by Nestor et al. (2008) in their sample of DLAs at $0.6 \leq z \leq 1.3$ and consistent with some of the rare strong Ca II absorbers in the sample of Wild & Hewett (2005).

We detected 21-cm absorption at the expected redshifted frequency towards this QGP from the data obtained on 2008 March 03. In order to obtain better S/N and rule out the possibility of weak RFI mimicking the absorption feature, the object was reobserved on 2009 June 13 and 2009 June 14. These repeat observations resulted in the absorption feature consistent with the spectrum from the earlier observations and the velocity shift expected from the heliocentric motion of the earth. The GMRT image overlaid on the SDSS r -band image and the 21-cm absorption spectrum towards the quasar are presented in Figs. 5 and 6 respectively. The spectrum presented in Fig. 6 is obtained after combining the different epoch spectra. The absorption profile is well modelled with the three distinct Gaussian components A, B and C (Fig. 6). The velocity offset of $\sim 10 \text{ km/s}$ between the strongest 21-cm absorption component and the redshift estimated from emission lines is within the redshift-measurement error. For a Gaussian profile, $N(\text{H I})$ and the peak optical depth (τ_p) are related by,

$$N(\text{H I}) = 1.93 \times 10^{18} \tau_p \frac{T_s}{f_c} \Delta v \text{ cm}^{-2}. \quad (4)$$

Here, τ_p , Δv and f_c are the peak optical depth, the FWHM in km s^{-1} of the fitted Gaussian, and the fraction of absorbing cloud covered by the radio source respectively. Individual Gaussian fits and fit parameters are presented in Table 4. The integrated 21-cm optical depth yields $N(\text{H I}) = 5.3 \times 10^{18} T_s \text{ cm}^{-2}$. If $T_s = 100 \text{ K}$, as usually seen in the case of cold neutral medium, then $N(\text{H I})$ will be $5 \times 10^{20} \text{ cm}^{-2}$. This is very close to the value we get from SED fitting using the Milky way extinction curve.

In the GMRT image there are two faint radio components, one to the east (referred to as J1241+6332E) and

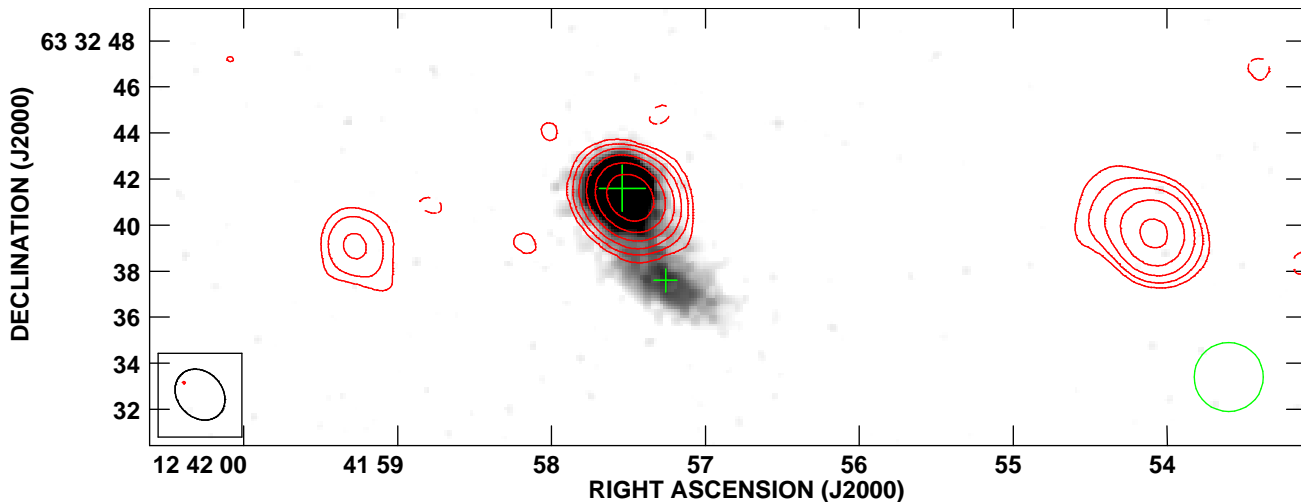


Figure 5. GMRT (contours) image overlaid on the SDSS *r*-band image of the quasar ($z_q = 2.625$ SDSS J124157.54+633241.6)–galaxy ($z_g = 0.143$ SDSS J124157.26+633237.6) pair. The radio image has an rms of $0.4 \text{ mJy beam}^{-1}$ and the restoring beam of $2.4'' \times 2.0''$ with the P.A. = 42° . The contour levels are $1.3 \times (-1, 1, 2, 4, 8, 16, 32) \text{ mJy beam}^{-1}$. The restoring beam for the radio image is shown as an ellipse and the optical positions of the quasar and the galaxy are marked with a big and a small cross respectively. The extent of the SDSS spectroscopic fiber is shown at the bottom right corner of the image.

Table 4. Details of the multiple Gaussian fits to the 21-cm absorption detected towards the quasar ($z_q = 2.625$ SDSS J124157.54+633241.6)–galaxy ($z_g = 0.143$ SDSS J124157.26+633237.6) pair.

Component [†]	z_{abs}	Δv^a	τ_p^b	$\frac{f_c N(H I)^c}{T_s}$
A	0.14294	10 ± 1	0.148 ± 0.010	0.29 ± 0.03
B	0.14285	16 ± 2	0.060 ± 0.007	0.19 ± 0.03
C	0.14303	11 ± 4	0.025 ± 0.009	0.05 ± 0.02

[†] components as indicated in Fig. 6

^a FWHM in km s^{-1} ; ^b peak optical depth

^c in units of 10^{19} cm^{-2}

one to the west (referred to as J1241+6332W) of the quasar (Fig. 5). It is not obvious if these radio components are associated with the quasar. No 21-cm absorption was detected towards J1241+6332E and J1241+6332W (see bottom panels of Fig. 8) at an angular separation of $13.6''$ and $21.2''$ respectively from the galaxy (Table 2). The flux density of these radio components is low and this prevents us from getting any useful constraint on the 21-cm optical depth towards these sight lines.

3.2 Details of QGPs with 21-cm absorption non-detections

Here we discuss the QGPs that do not show any detectable 21-cm absorption. The color representations of these 4 QGPs are presented in Fig. 7. The lack of 21-cm absorption could be either related to low column density of H I along the sight line and/or high spin-temperature, T_s . If a sight line passes through either the optical disk or an extended H I 21-cm line emitting region then one is sure of having sufficient H I column density. For our sample we shall use Petrosian radius (R_{90}) containing 90% of the Petrosian flux measured using *r*-band SDSS images as an indicator of optical ex-

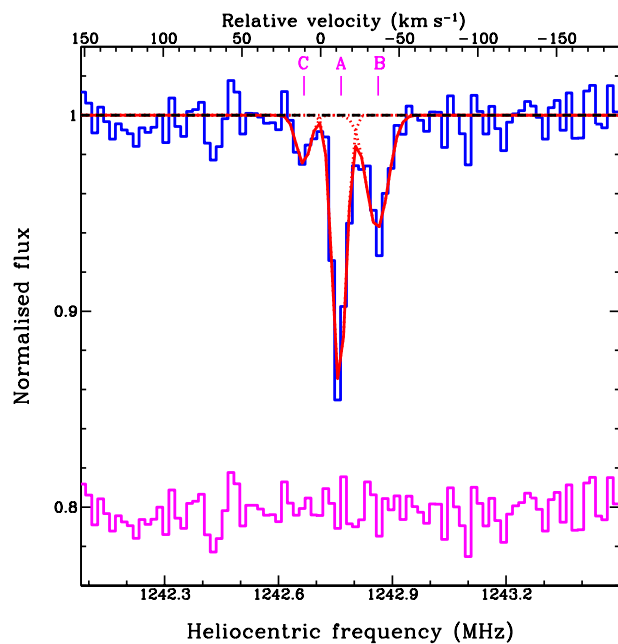


Figure 6. GMRT spectrum of the 21-cm absorption detected towards the quasar ($z_q = 2.625$ SDSS J124157.54+633241.6)–galaxy ($z_g = 0.143$ SDSS J124157.26+633237.6) pair. Zero of the velocity scale is defined at $z_{em} = 0.14299$ determined from the nebular emission detected in the SDSS spectrum. Individual Gaussian components and the resultant fits to the absorption profile are plotted as dotted and continuous lines respectively. Residuals, on an offset arbitrarily shifted for clarity, are also shown.

tent. These values are given in Table 2 for all the galaxies in our sample. The extent of the H I gas in these galaxies is not known. So we use the existing correlations between optical properties and H I radius, (R_{HI}), found for the local galaxies. In the local universe, R_{25} (the distance along the

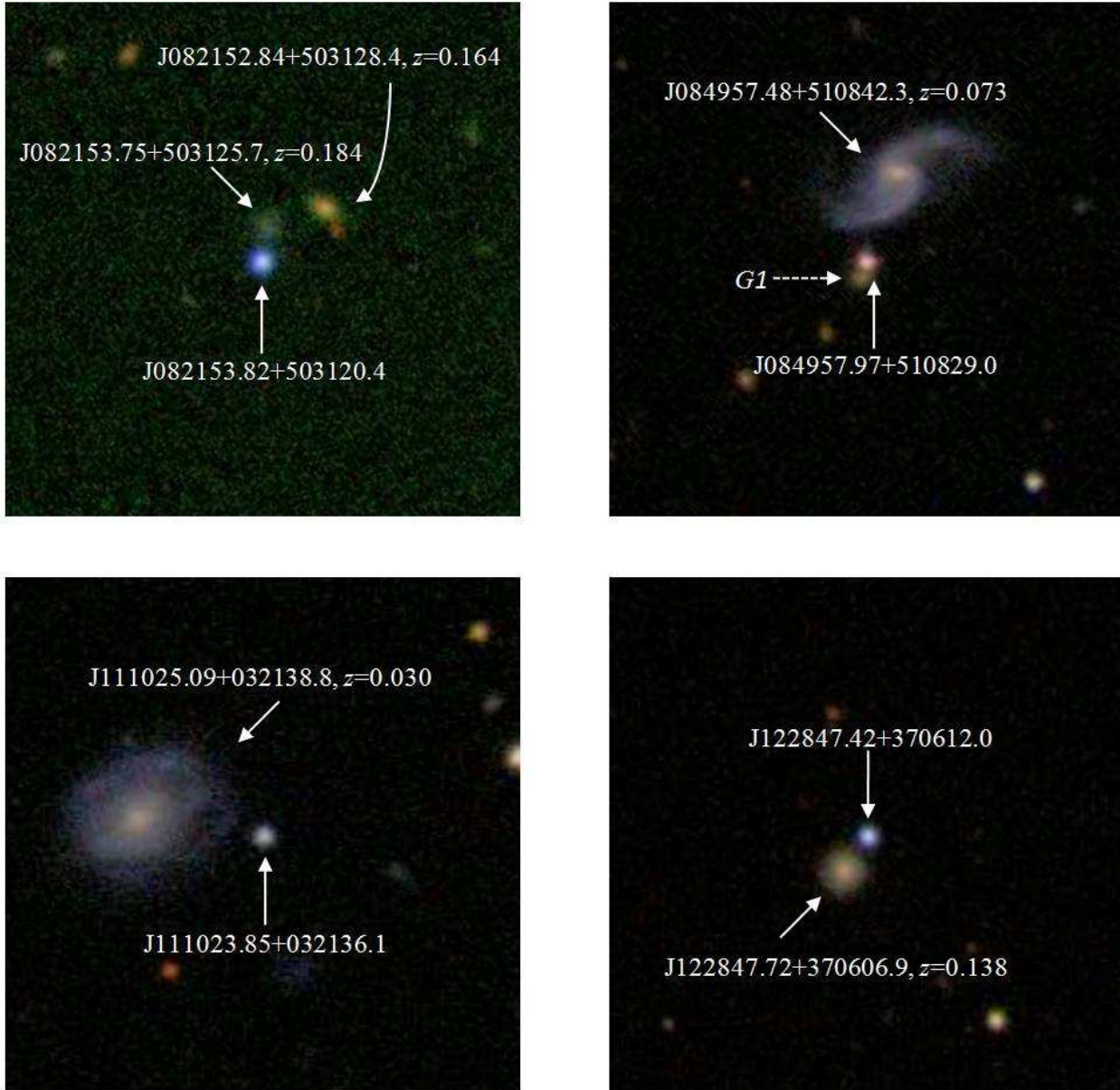


Figure 7. Color representations of the QGPs with no 21-cm absorption detections (see Section 3.2). Each image is $77''$ on a side, with north-east towards the top left corner, and centered on the QSO. Galaxies with known redshifts are identified, along with their corresponding redshifts. In the field of QSO J084957.97+510829.0 (top right panel), the object labeled “G1” is the galaxy we suggest is responsible for the Ca II and Na II absorption at $z_g = 0.3120$, discussed in Section 3.2.2.

semi-major axis where the B-band surface brightness falls to $25 \text{ mag arcsec}^{-2}$) is used to quantify the optical radius of the galaxies. It is also known that the extent of H I gas as measured from the 21-cm emission maps with 1σ column density of few times 10^{19} cm^{-2} is roughly 1.7 times R_{25} (No-ordermeer et al. 2005). As the scaling is found not to depend strongly on the galaxy morphology (see Fig. 3 of Broeils & Rhee 1997) we use this for all the galaxies. Whenever possible we perform isophotal analysis using ellipse fitting to get R_{25} and the extent of H I gas, R_{HI} .

As the galaxies in our sample are at higher redshifts (i.e. $z \geq 0.03$) any weak dependence of R_{HI} on the absolute magnitude should also be considered. Therefore, we also obtain R_{HI} using absolute B-band magnitude and Equation 2 of

Lah et al. (2009) derived from various correlations found by Broeils & Rhee (1997). We get the B-band magnitude using r - and g -band magnitudes of the galaxy measured in the SDSS images and the filter transformation equations given by Lupton (2005)¹. The above two estimates of R_{HI} allow us to have a rough idea of possible H I extent in these galaxies. In what follows we discuss each QGP in detail.

¹ <http://www.sdss.org/dr6/algorithms/sdssUBVRITransform.html>

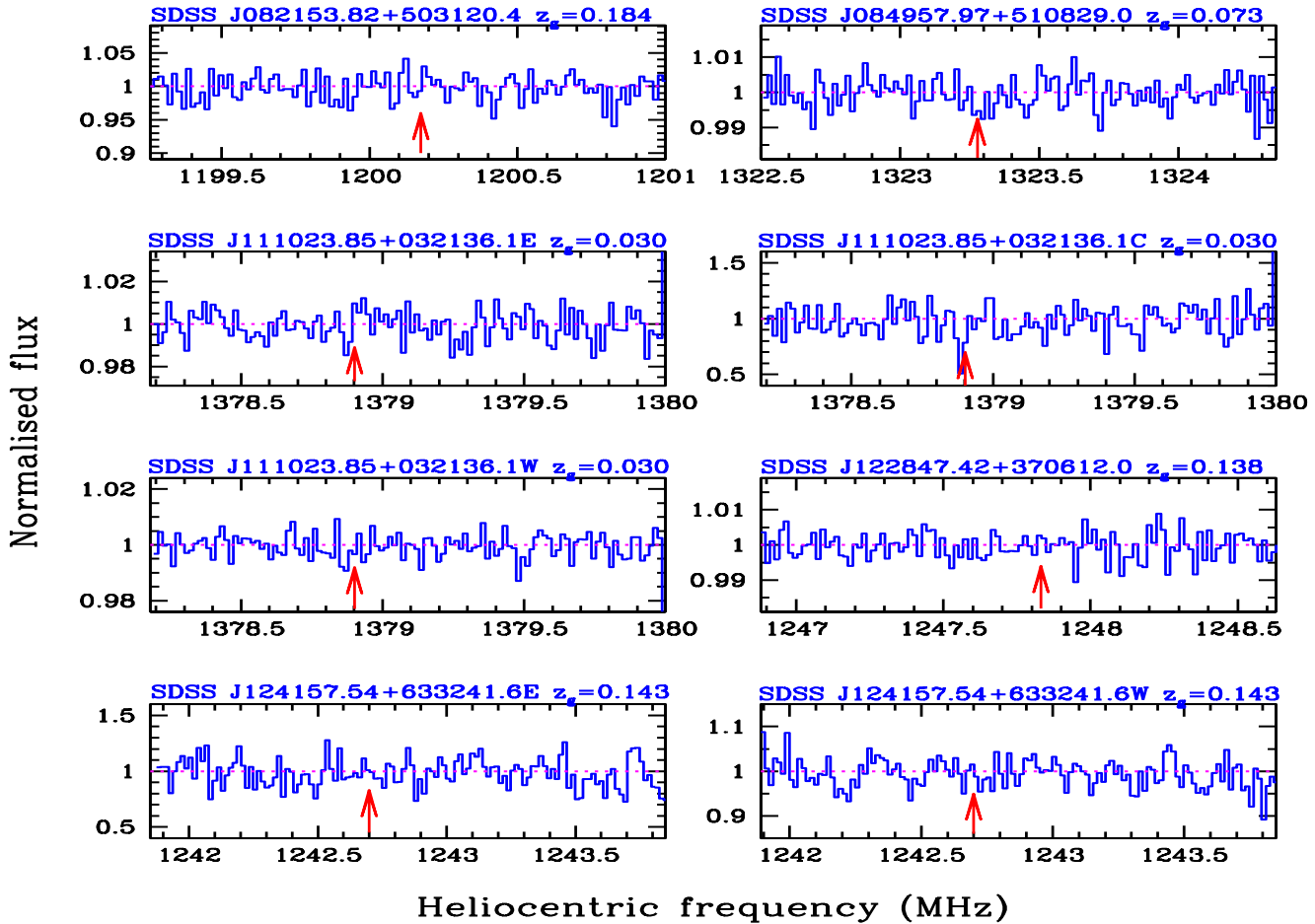


Figure 8. GMRT spectra of QGPs with 21-cm absorption non-detections. Arrows mark the expected position of 21-cm absorption lines based on the galaxy redshift.

3.2.1 Quasar ($z_q = 2.130$ SDSS J082153.82+503120.4) – galaxy ($z_g = 0.184$ SDSS J082153.75+503125.7) pair

The background quasar J082153.82+503120.4 has a flux density of ~ 54 mJy in the 1.4 GHz FIRST image and is the weakest background radio source in our sample of QGPs to search for 21-cm absorption. The SDSS r -band image shows that there are two galaxies within $0.2'$ of the quasar. The nearest of these i.e. J082153.75+503125.7 is at a separation of $5.2''$ whereas the other galaxy i.e. J082152.84+503128.4 is at the distance of $12.2''$ (see top left panel of Fig. 7).

We measured the redshift of the galaxy J082153.75+503125.7 using our APO spectrum to be $z_g=0.1835$. (Fig. 9). Data were taken on 2007 March 14 using DIS at APO, with the B400/R300 grating, with a $1.5''$ slit and the exposure time was 1200 sec. While obtaining the spectrum of the closest galaxy (J082153.75+503125.7), the DIS slit was orientated to also cover the second galaxy i.e. J082152.84+503128.4. The spectrum of the second galaxy showed no emission lines, but strong Ca II H & K, G-band, and Na I stellar absorption lines. To calculate the redshift of this galaxy, we used the IRAF routine `fxcor` to cross-correlate its spectrum with that of a Galactic star

with a known radial velocity, HD 182572. We derived a redshift of $z = 0.1640$, with an error of $\simeq 200$ km s $^{-1}$. In this case, the error is dominated by the error given by `fxcor`, which is larger than the error from the wavelength calibration of the spectrum itself. We searched for 21-cm absorption only in the galaxy SDSS J082153.75+503125.7 at $z_g=0.184$ and do not discuss the second galaxy hereafter.

The galaxy J082153.75+503125.7 is faint ($M_B = -19.1$ mag and $L/L_B^* = 0.19$ if we use $M_B^* = -20.90$ as found by Marinoni et al. 1999) and compact with $R_{90} \sim 3.5''$ with a corresponding physical extent of 10.7 kpc. We estimate the effective H I radius R_{HI} of 8.2 kpc from the B-band absolute magnitude. As the object is faint we could not perform isophotal analysis for this galaxy. However, it is clear that optical extent and estimated H I radius are significantly smaller than the impact parameter of the galaxy from the QSO sight line (i.e 15.9 kpc).

In the SDSS QSO spectrum we do not find Ca II and Na I absorption at the z_g . The 3σ upper limit for $W_r(\text{Ca II } \lambda 3935)$ is 0.25 \AA . The spectral energy distribution of the QSO is also consistent with very little reddening. Based on the SED fits we find $\tau_V = 0.10 \pm 0.02$ and $E(B-V) = 0.04 \pm 0.01$. The GMRT image overlaid on the SDSS r -band image is presented in Fig. 10. No 21-cm absorption is de-

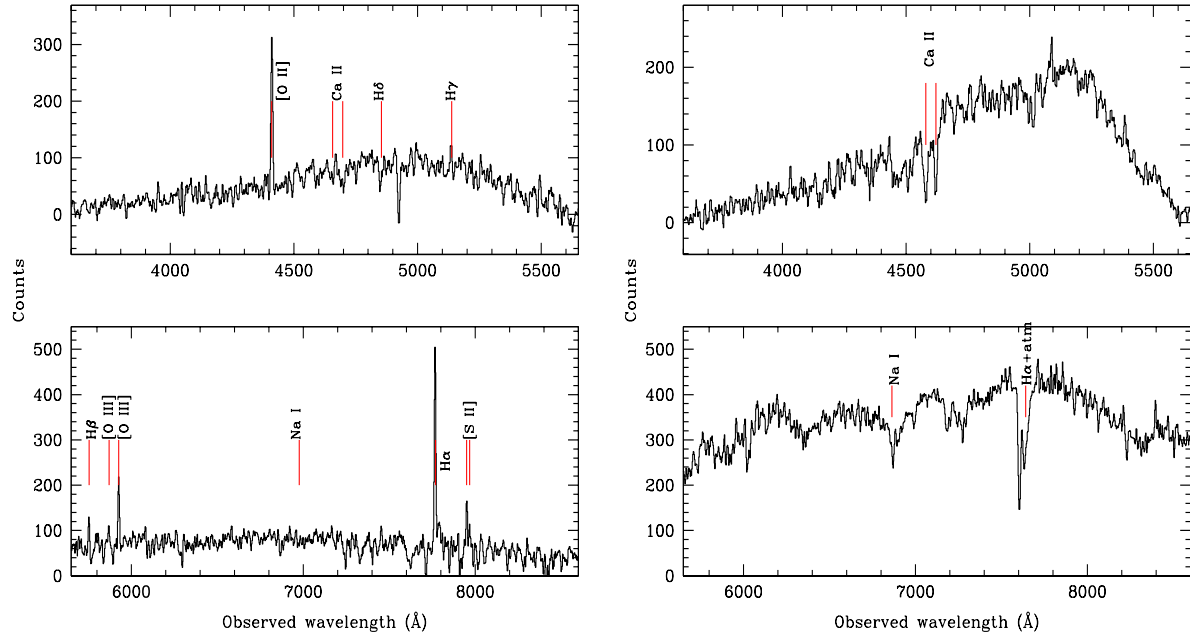


Figure 9. APO spectrum of the galaxy J082153.75+503125.7 at $z_g = 0.1835$ (left) and J082152.84+503128.4 at $z_g = 0.1640$ (right).

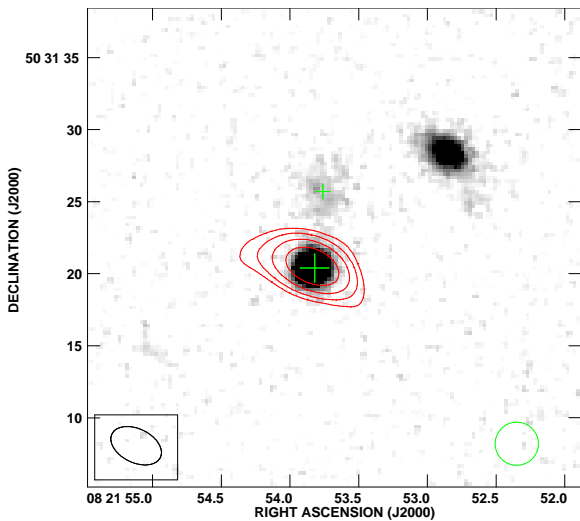


Figure 10. GMRT (contours) image overlaid on the SDSS r -band image of the quasar ($z_q = 2.130$ SDSS J082153.82+503120.4) – galaxy ($z_g = 0.184$ SDSS J082153.75+503125.7) pair. The radio image has an rms of $0.2 \text{ mJy beam}^{-1}$ and the restoring beam of $3.7'' \times 2.3''$ with the P.A.= 64.0° . The contour levels are $2.1 \times (-1, 1, 2, 4, 8) \text{ mJy beam}^{-1}$. The restoring beam for the radio image is shown as an ellipse and the optical positions of the quasar and the galaxies are marked with the big and small crosses respectively. The extent of the SDSS spectroscopic fiber is shown at the bottom right corner of the image.

tected towards this radio source at the impact parameter of 15.9 kpc (Fig. 8). The 3σ upper limit on the H I column density is $N(\text{H I}) = 7.0 \times 10^{17} \text{ T}_S \text{ cm}^{-2}$. As the impact parameter is larger than optical radius and the H I radius estimated above the lack of absorption could be simply due to the lack of sufficient neutral gas along the line of sight.

3.2.2 Quasar ($z_q = 0.584$ SDSS J084957.97+510829.0) – galaxy ($z_g = 0.073$ SDSS J084957.48+510842.3) pair

The background radio source is a well-known object which has a BL Lacertae spectrum during outbursts (Arp et al. 1979). The redshift of this object was measured to be $z_q = 1.860$ on the basis of the two emission lines which were identified as $\text{CIV} \lambda 1549$ and $\text{CIII} \lambda 1909$ (Arp et al. 1979). The actual redshift as estimated from the SDSS spectrum with much wider spectral coverage detecting the emission lines of Mg II , O[III] , $\text{H}\beta$, $\text{H}\gamma$ and $\text{H}\delta$ has been found to be $z_{\text{em}} = 0.584$. The radio source is situated at $14.1''$ south of the galaxy J084957.48+510842.3 at $z_g = 0.073$ which is the southern member of the interacting pair of galaxies (Stickel, Fried & Kühr 1989). This is the brightest galaxy in our sample ($M_B = -20.7$ and $L_B/L_B^* = 0.8$). Based on the absolute B-band magnitude we expect the H I emission to extend up to a radius of 14 kpc . We used the redshift of $z_g = 0.0734$ (measured from the SDSS spectrum of the galaxy) to search for 21-cm absorption from the halo of foreground spiral galaxy. The GMRT image overlaid on the SDSS r -band image is shown in Fig. 11. The radio source is compact in our image and no 21-cm absorption was detected towards this sight line at $z_g = 0.0734$ with the impact parameter of 19.4 kpc (Fig. 8). The corresponding 3σ upper limit on the H I column density is $N(\text{H I}) = 1.5 \times 10^{17} \text{ T}_S \text{ cm}^{-2}$.

This QGP has been previously searched for 21-cm absorption and molecular absorption by Boissé et al. (1988) and Wiklind & Combes (1995) respectively. Boissé et al. (1988) obtained a shallower spectrum of this radio source using the Nançay radio telescope yielding 3σ 21-cm optical depth limit, $\int \tau_{3\sigma} dv < 0.32 \text{ km s}^{-1}$ as compared to the limit of 0.08 km s^{-1} presented here. Absorption lines of Ca II and Na I are not detected in the SDSS QSO spectrum. However,

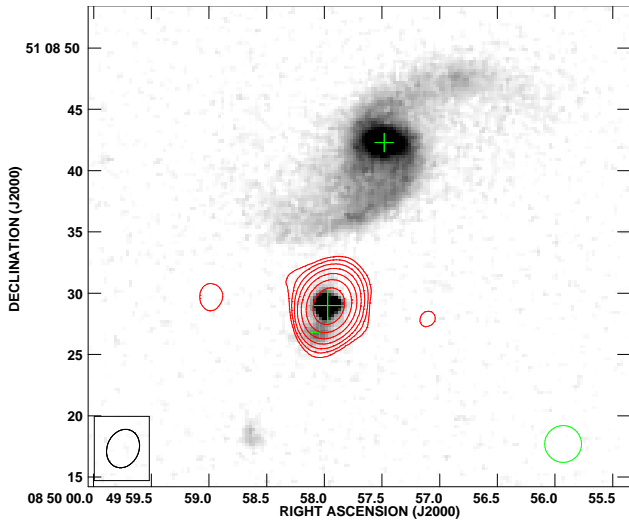


Figure 11. GMRT (contours) image overlaid on the SDSS r -band image of the quasar ($z_q = 0.584$ SDSS J084957.97+510829.0) – galaxy ($z_g = 0.073$ SDSS J084957.48+510842.3) pair. The radio image has an rms of $0.4 \text{ mJy beam}^{-1}$ and the restoring beam of $3.2'' \times 2.6''$ with the P.A. = -22.6° . The contour levels are $2.1 \times (-1, 1, 2, 4, 8, 16, 32, 64, 128) \text{ mJy beam}^{-1}$. The restoring beam for the radio image is shown as an ellipse and the optical positions of the quasar and the galaxy are marked with a big and a small cross respectively. The extent of the SDSS spectroscopic fiber is shown at the bottom right corner of the image.

since quasar is faint, the equivalent width upper limits are poor (Table 2).

There are speculations about the optical spectrum of this blazar being affected by foreground galaxy lensing and/or reddening (Stickel et al. 1989; Ostman 2006). It is known that dusty absorbers tend to show strong 21-cm absorption (cf. Srianand et al. 2008 and the detection presented in Section 3.1). The absence of 21-cm absorption is thus inconsistent with the dust reddening observed in the spectrum of the QSO by the galaxy J084957.97+510829.0. If we use the average spin temperature of 500 K measured in the QGPs (Carilli & van Gorkom 1992), our observations are consistent with $N(\text{H I}) \leq 7.5 \times 10^{19} \text{ cm}^{-2}$. This is too low to produce any detectable extinction even if the dust-to-gas ratio is close to what we see in the Milky way.

We have detected strong Na I and Ca II absorption at $z_{\text{abs}}=0.3120$ towards this quasar sight line through our APO 3.5-metre observations on 2007 May 22 (Fig. 12). These observations used DIS R1200/B1200 gratings with a $1.5''$ slit and the exposure time was $3 \times 1500 \text{ sec}$. Rest frame equivalent widths for Na I and Ca II absorption lines are $W_r(\text{Na I } \lambda 5889) = 0.84 \pm 0.25$, $W_r(\text{Na I } \lambda 5895) = 0.60 \pm 0.22$, $W_r(\text{Ca II } \lambda 3935) = 0.60 \pm 0.18$ and $W_r(\text{Ca II } \lambda 3970) = 0.39 \pm 0.16$. It is possible that this strong Ca II absorber originates from the galaxy (labelled ‘G1’) blended with quasar in the SDSS image (Fig. 7) and is responsible for the reddening of quasar. Unfortunately, the GMRT data to search for 21-cm absorption in this system were rendered unusable due to strong RFI.

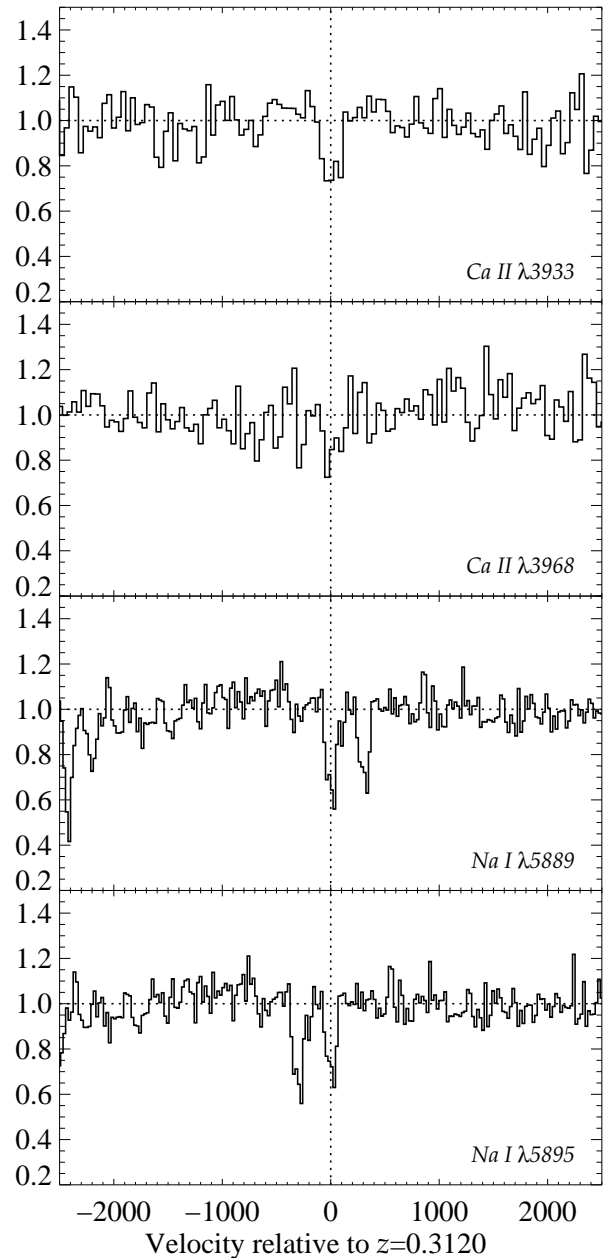


Figure 12. Velocity plot for the Na I and Ca II absorption lines (wavelengths are in air) detected towards the quasar, SDSS J084957.97+510829.0.

3.2.3 Quasar ($z_q = 0.966$ SDSS J111023.85+032136.1) – galaxy ($z_g = 0.030$ SDSS J111025.09+032138.8) pair

Murdoch et al. (1983) presented detailed spectroscopy of the background quasar as well as the foreground galaxy that has been classified as Sc. This is the lowest redshift galaxy in our sample. The SDSS quasar spectrum does not show Ca II absorption lines at the redshift of the galaxy. The radio emission from the quasar is well resolved into a triple in our GMRT image where most of the emission is contained in the two lobes on either side of the foreground galaxy (Fig. 13). The radio lobe to the west of the foreground galaxy is at a

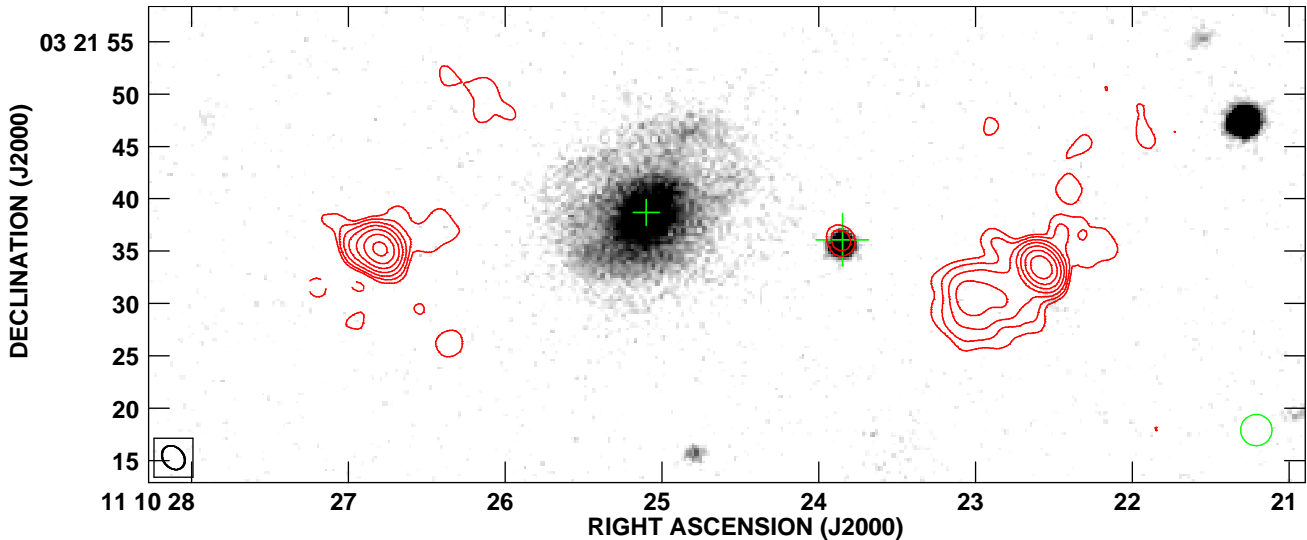


Figure 13. GMRT (contours) image overlaid on the SDSS r -band image of the quasar ($z_q = 0.966$ SDSS J111023.85+032136.1) – galaxy ($z_g = 0.030$ SDSS J111025.09+032138.8) pair. The radio image has an rms of $0.4 \text{ mJy beam}^{-1}$ and the restoring beam of $2.5'' \times 1.9''$ with the P.A. = 40° . The contour levels are $2.0 \times (-1, 1, 2, 4, 8, 16, 32, 64) \text{ mJy beam}^{-1}$. The restoring beam for the radio image is shown as an ellipse and the optical positions of the quasar and the galaxy are marked with a big and small a cross respectively. The extent of the SDSS spectroscopic fiber is shown at the bottom right corner of the image.

projected separation of $\sim 25.7''$ (15.3 kpc) whereas the radio lobe towards the east is at the angular separation of $\sim 37.9''$ (22.5 kpc). The radio core is at the separation of $18.8''$ from the galaxy but is unfortunately very weak with the peak flux density of only $7.6 \text{ mJy beam}^{-1}$. The radio source therefore provides multiple sight lines close to the foreground galaxy. The galaxy has Petrosian radius $R_{90} \sim 11.74''$. We use the r - and g -band SDSS images and ellipse fitting routine in STSDAS package in IRAF to get the surface brightness profile of the galaxy (see Fig 14). We get R_{25} , the radius at which the B-band surface brightness reaches $25 \text{ mag arcsec}^{-2}$, using these profiles and $B = g + 0.3130(g - r) + 0.2271$. This together with the well known relationship between the radius of the H I emitting gas and R_{25} measured for Sa/Sab galaxies (Noordermeer et al. 2005) we expect the H I gas to extend upto $17''$ (i.e $\sim 10 \text{ kpc}$) from the center of the galaxy. The absolute B-band magnitude of this galaxy is -18.6 mag and $L_B/L_B^* = 0.12$. The R_{HI} expected from the absolute B-band magnitude is 6.8 kpc . Therefore, if this galaxy follows standard scaling relation assumed here we expect only the sight line towards the radio core to pass through the H I disk.

No 21-cm absorption was detected towards any of the radio components. The absorption spectra towards the peak components of the eastern and western radio lobes (referred to as J1110+0321E and J1110+0321W) and the radio core (i.e. J1110+0321C) are presented in the Fig. 8 and the corresponding optical depth limits are provided in the Table 2. In the case of the core, the sight line may just graze through the outer H I disk. But due to the weakness of radio emission, the 21-cm absorption optical depth limit is very high. The integrated optical depths typically seen in the QGPs are much lower than this limit (see Section 4.1). The best 3σ upper limit on the H I column density, $N(\text{H I}) = 1.5 \times 10^{17} \text{ T}_{\text{S}} \text{ cm}^{-2}$, is obtained towards the J1110+0321W component.

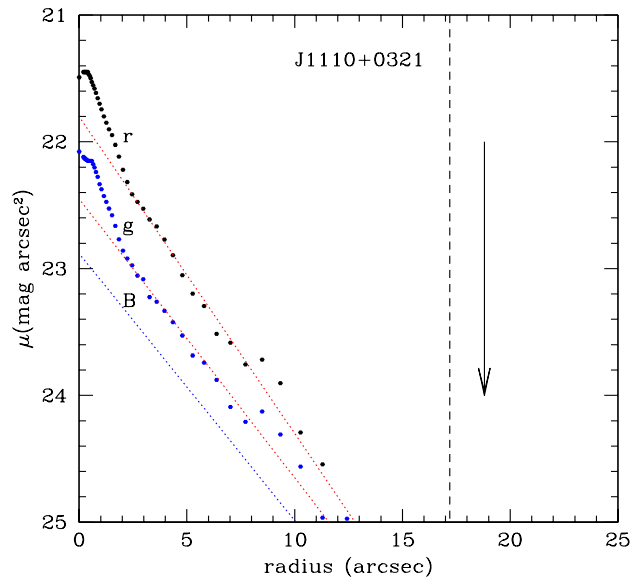


Figure 14. The r - and g -band surface brightness profile of the galaxy J111025.09+032138.8 with best fitted exponential profiles over-plotted. We construct the B-band surface brightness profile using $B = g + 0.3130(g - r) + 0.2271$ and estimate R_{25} . The vertical dashed line marks the expected radius of the H I gas based on the relationship between H I radius and R_{25} obtained by Noordermeer et al. (2005). The arrow marks the impact parameter for the core of the QSO.

3.2.4 Quasar ($z_q = 1.517$ SDSS J122847.42+370612.0) – galaxy ($z_g = 0.138$ SDSS J122847.72+370606.9 pair):

The foreground galaxy at the redshift of 0.1383 is at the projected separation of ($6.2''$) 15 kpc (Fig. 15). The galaxy

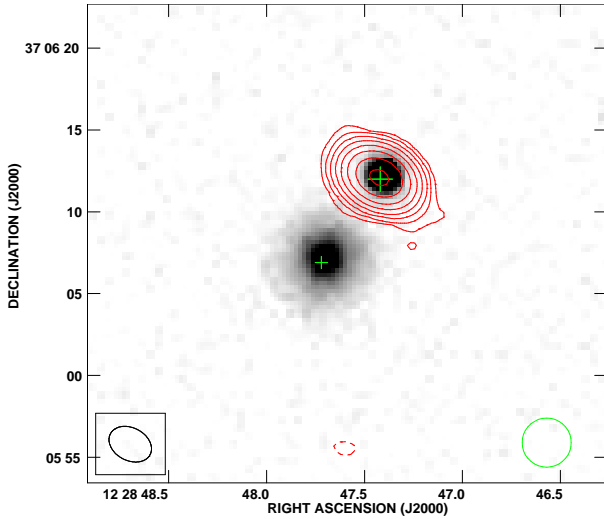


Figure 15. GMRT (contours) image overlaid on the SDSS r -band image of the quasar ($z_q = 1.517$ SDSS J122847.42+370612.0) – galaxy ($z_g = 0.138$ SDSS J122847.72+370606.9) pair. The radio image has an rms of $0.4 \text{ mJy beam}^{-1}$ and the restoring beam of $2.7'' \times 2.0''$ with the P.A. = 62° . The contour levels are $2.1 \times (-1, 1, 2, 4, 8, 16, 32, 64, 128) \text{ mJy beam}^{-1}$. The restoring beam for the radio image is shown as an ellipse and the optical positions of the quasar and the galaxy are marked with a big and a small cross respectively. The extent of the SDSS spectroscopic fiber is shown at the bottom right corner of the image.

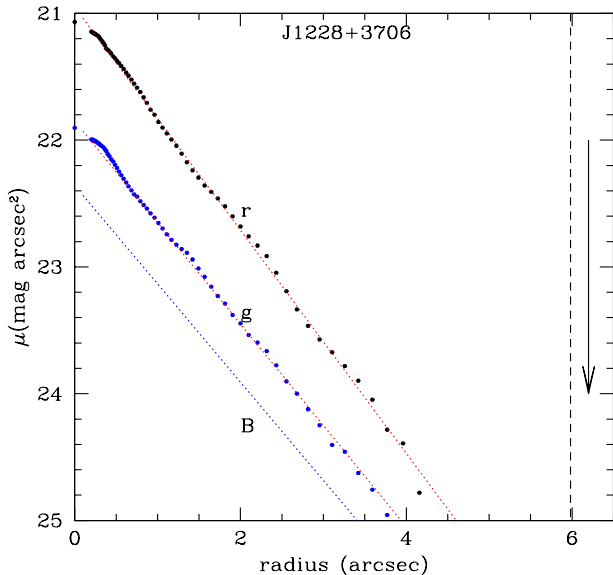


Figure 16. The r - and g -band surface brightness profile of the galaxy J122847.72+370606.9 with best fitted exponential profiles over-plotted. Rest are similar to that of Fig. 14.

in this case is face-on with $R_{90} = 4.4''$. We also performed the ellipse fitting to this galaxy and estimated the possible extent ($R_{\text{H I}} = 14 \text{ kpc}$) of H I gas in this galaxy (Fig. 16). The absolute B-band magnitude of the galaxy is -19.9 mag and L_B/L_B^* is 0.41. We derive $R_{\text{H I}} = 11 \text{ kpc}$ from the absolute B-band magnitude. This suggests that the QSO sight line may just graze through the

outer part of the extended H I gas. The redshift of the galaxy is accurately measured from the available SDSS spectrum of the galaxy. Weak absorption features with rest equivalent widths $W_r(\text{Ca II } \lambda 3935) = 0.49 \pm 0.13 \text{ \AA}$ and $W_r(\text{Ca II } \lambda 3970) = 0.20 \pm 0.13 \text{ \AA}$ are detected at the expected positions of Ca II doublet in the SDSS QSO spectrum. However, Na I absorption lines are not detected. The GMRT image overlaid on the SDSS r -band image is presented in Fig. 15. No 21-cm absorption is detected towards this QGP (Fig. 8) with the 3σ upper limit on the H I column density being $N(\text{H I}) = 1.3 \times 10^{17} \text{ T}_S \text{ cm}^{-2}$.

4 DISCUSSION

In order to investigate the relationship between 21-cm absorption and the properties of the absorbing galaxy, we combine our results with 21-cm absorption measurements of all the QGPs available in the literature (Table 5). Observations of the QGP 3C268.4/NGC4138 available from Haschick, Crane & Baan (1983) are not considered here. In this case, 21-cm absorption superimposed on the 21-cm emission is inferred from the sharp interruption in the emission profile obtained using Green Bank 300-ft antenna and the absorption optical depth is highly uncertain. In addition to this list, 21-cm absorption has been detected towards the radio source 3C178 from the foreground galaxy NGC2377 (Haschick et al. 1980). The nature of background source is not clear in this case. Radio source is resolved into two components with linear angular size of $24''$ and 21-cm absorption is detected towards both the northern and southern components which are at impact parameters of 4.1 kpc and 7.4 kpc respectively. We denote such pairs as RGPs and these are not considered here. In the following we discuss the properties of sight lines searched for 21-cm absorption as part of the observations of QGPs and investigate their relationship with the high- z 21-cm absorbers detected in the Mg II absorbers and DLAs towards quasars.

4.1 Impact parameter

In Fig. 17, we plot 21-cm integrated optical depth as a function of impact parameter for all the sight lines from the samples of QGPs (Tables 2 and 5) with impact parameters less than 30 kpc. We do not find any correlation between the optical depth and impact parameter.

We estimate the filling factor of 21-cm absorbing gas for a limiting integrated 21-cm optical depth $\mathcal{T}_{21} (= \int \tau dv)$. When we consider QGPs with impact parameter less than 15 kpc, we have 5 detections out of 10 sight lines where $\mathcal{T}_{21} \geq 0.1 \text{ km s}^{-1}$. Thus the detectability of 21-cm absorption with $\mathcal{T}_{21} \geq 0.1 \text{ km s}^{-1}$ is $\sim 50\%$. This limiting value of \mathcal{T}_{21} corresponds to $\log N(\text{H I}) = 19.3$, if the spin temperature of the gas is 100 K as expected in the case of cold neutral medium. However, the measured spin temperatures in the case of QGPs are usually in the range 200 K to 900 K (see Table 3 of Carilli & van Gorkom 1992). So if we take a typical value of 500 K for the T_S then the limiting column density of H I is $\log N(\text{H I}) = 20.0$. Thus $\mathcal{T} \geq 0.1 \text{ km s}^{-1}$ limit will be sensitive to detecting similar gas clouds in high redshift DLAs.

Using 21-cm emission line maps of nearby galaxies,

Table 5. Quasar-galaxy pairs with 21-cm absorption measurements from the literature arranged in the order of increasing galaxy redshift.

Quasar/galaxy pair	z_q	z_g	Angular Separation	Distance	$\int \tau dv$	Ref.	$W_r(\text{Ca II}\lambda 3935)$
(1)	(2)	(3)	($''$) (4)	(kpc) (5)	(6)	(7)	(8)
Detections							
3C232/NGC3067	0.530	0.0049	110.6	11.1	0.11	1	$0.43\pm 0.05^+$
Q1327–206/1327-2041	1.169	0.0180	38.5	13.9	0.14^\dagger	1	$0.58\pm 0.04^*$
Q2020–370/Klemola 31A	1.048	0.0270	18.7	10.0	0.22	1	$0.35\pm 0.08^*$
J104257.58+074850.5/ J104257.74+074751.3	2.665	0.0332	2.5	1.7	0.19	2	$<1.07^{**}$
Q0248+430/Anon	1.313	0.0520	15.0	15.0	0.26	3	$1.52\pm 0.17^*$
Non-detections							
1749+70.1/NGC6503	0.770	0.0002	321.6	10.3	$<0.10^\ddagger$	4	–
3C309.1/NGC5832	0.905	0.00149	372.0	11.2	<0.014	5	–
H0131+154/NGC628	1.330	0.0022	2188.9	94.1	<0.148	6	–
3C275.1/NGC4651	0.555	0.0027	220.3	12.1	<0.010	6	$<0.45^{**}$
0139+132/NGC660	0.267	0.0028	911.1	51.9	<0.067	6	$<0.45^{**}$
2304+32B/NGC7490	1.937	0.0207	495.8	204.8	<0.10	6	–
3C455/NGC7413	0.543	0.0325	23.4	14.9	<0.026	6	–
2231+0953/UGC12081	1.854	0.0388	121.6	92.3	<0.10	6	–
Q0446–208/Anon	1.894	0.0661	12.3^C	15.4	<0.21	1	$0.57\pm 0.06^*$
			29.6^E	37.1	<0.32		–
			28.1^W	35.2	<0.63		–

Column 1: Quasar/galaxy pair. Column 2: Quasar redshift. Column 3: Galaxy redshift. Column 4 and 5: Angular separation and the projected separation of quasar/radio component from the centre of galaxy. The superscripts *C*, *E* and *W* correspond to core, eastern and western components respectively. Column 6: Integrated 21-cm optical depth or 3σ upper limit in case of non-detections with data smoothed to 10 km s^{-1} . Column 7: Reference for the 21-cm optical depth value or upper limit. Column 8: Rest equivalent width of Ca II or 3σ upper limit to it.

† 21-cm absorption is detected in two well-detached components separated by $\sim 250 \text{ km s}^{-1}$. The integrated 21-cm optical depth presented here corresponds to the stronger component (see text for details).

$^\ddagger \Delta v = 20.6 \text{ km s}^{-1}$.

$^+$ $W_r(\text{Ca II})$ taken from Bowen et al (1991).

* $W_r(\text{Ca II})$ taken from Womble (1993).

** $W_r(\text{Ca II})$ estimated from the SDSS spectrum.

References for the H I absorption data– 1: Carilli & van Gorkom (1992); 2: Borthakur et al. (2010); 3: Hwang & Chiou (2004); 4: Boissé et al. (1988); 5: Haschick & Burke (1975) and 6: Corbelli & Schneider (1990).

Zwaan et al. (2005) have concluded that sight lines with $\log N(\text{H I}) \geq 20.3$ occur with a median impact parameter of 7.8 kpc. It is also clear from their Fig. 14 that when the impact parameter is between 10 and 15 kpc, the probability of having high $N(\text{H I})$ is roughly between 50% to 70%. This is very much consistent with what we find here.

4.2 Extent of the H I disk of galaxy

In the previous sub-section we do not consider the possibility that the 21-cm absorption non-detection may simply be due to the small H I extent of the galaxy. As discussed before, the expected extent of H I gas in all but one of the galaxies in our sample (Table 2) with no 21-cm detection is smaller than the impact parameter. The only case (J124157.54+633241.6) where we have 21-cm detection is when the radio sight line is passing through the stellar disk (as we detect emission lines from the galaxy in the QSO spectrum).

Amongst the QGPs with 21-cm detections from the literature (Table 5), in the three cases i.e. 3C 232/NGC3067,

Q 1327–206/1327–2041 and Q 2020–370/Klemola 31A, the quasar sight line passes through the H I emission disk of the foreground galaxy – a late type spiral – extending well beyond the stellar disk and also shows signs of tidal disturbances (Carilli & van Gorkom 1992). In the case of Q0248+430/G0248+430, the foreground galaxy is actually a pair of interacting luminous infrared galaxies. The QSO sight line in the optical image passes through the tidal tail extending in the direction of the background quasar (Womble et al. 1990; Hwang & Chiou 2004). No H I emission was detected from the foreground galaxy with a limiting hydrogen mass of $6 \times 10^8 M_\odot$. In the case of Quasar (J104257.58+074850.5) – galaxy (J104257.74+074751.3) pair, the QSO sight line passes through the optical disk of an H I deficient galaxy (Borthakur et al. 2010). Thus all the 21-cm absorption detections are associated with the quasar sight lines passing through the stellar and/or extended H I disk of the galaxy.

Let us now consider the 5 QGPs in Table 5 with impact parameters less than 20 kpc that do not show 21-cm

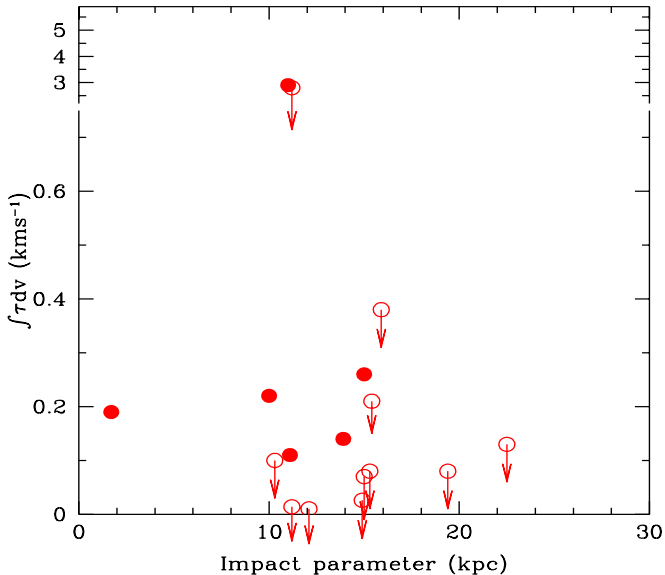


Figure 17. Integrated 21-cm optical depth is plotted against projected separation between the background radio source and the centre of galaxy (Tables 2 and 5). In case of non-detections values are 3σ upper limits corresponding to the equivalent velocity resolution of 10 km s^{-1} . Filled symbols are for the detections and open symbols are for the non-detections.

absorption. In the case of 1749+70.1/NGC6503 high signal-to-noise H I emission maps show extended H I emission along the semi-major axis (Greisen et al. 2009). The QSO sight line is at an impact parameter of 10.3 kpc along the minor axis and not passing through the H I disk. In the case of 3C275.1/NGC4651 the QSO sight line passes through the outer regions of the H I 21-cm emission disk (Schneider et al. 1993). There is a tentative detection of 21-cm absorption noted by Schneider et al. (1993). In the absence of further confirmation we have considered this case as a non-detection. In the case of 3C309.1/NGC5832 and 3C455/NGC7413 no radio interferometric 21-cm emission maps are available, whereas for the Q0446–208/Anon H I 21-cm emission is not detected. It is interesting to note that in case of Q0446–208/Anon the quasar sight line passes through the stellar disk of the galaxy (Carilli & van Gorkom 1992).

Thus it appears that the lack of 21-cm absorption in 50% of the cases with impact parameter less than 20 kpc could be related to the smaller extent of H I gas in galaxies and probably not related to the filling factor of cold gas in the extended H I disk/halo. Confirming this conclusion with a large number of QGPs with low impact parameter is important for our understanding of high- z 21-cm absorbers.

4.3 Ca II absorption

The presence of Ca II and/or Na I absorption can also be used as a tracer of neutral gas. Detecting significant amounts of these two species will ensure that the region probed is cold and relatively well shielded from the ionizing UV radiation. Wild et al. (2006) have detected several strong Ca II absorbers ($W_r(\text{Ca II } \lambda 3935) \geq 0.5 \text{ \AA}$) in the

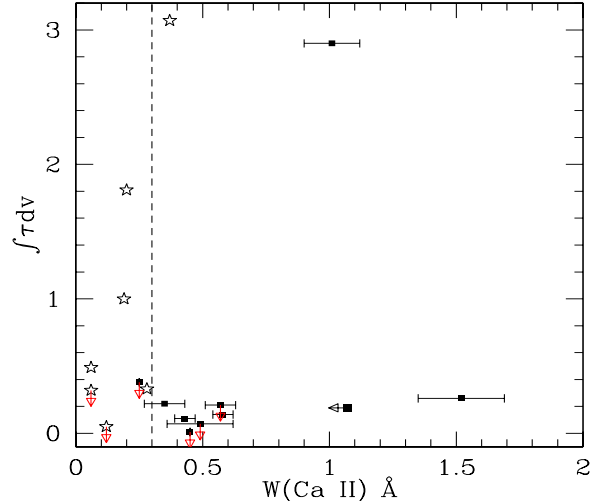


Figure 18. The integrated 21-cm optical depth is plotted against $W_r(\text{Ca II } \lambda 3935)$ for QGPs (squares) and for $z \leq 1$ DLAs (stars).

SDSS database. These absorbers are found to be *dustier* than the systems detected through the presence of Mg II absorption or DLA. Wild et al. (2007b) have detected strong nebular emission originating from the Ca II absorbers by stacking methods. All these suggest that the QSO sight lines with Ca II absorbers may be going very close to the star-forming regions. Indeed Zych et al. (2007) have detected galaxies associated with four strong Ca II absorbers with typical impact parameters less than 23 kpc. It is interesting to note that all the QGPs, except the J104257.58+074850.5/J104257.74+074751.3², that show 21-cm absorption also show Ca II and Na I absorption in the optical spectra. Bowen et al (1991) have found that Ca K line with a rest equivalent width $\geq 0.3 \text{ \AA}$ is detected only along sight lines with impact parameters less than 11 kpc. For the cosmological parameters used here this corresponds to ~ 15 kpc.

We have clear detections of Ca II in two out of 5 QSO sight lines in our sample. In the case of two QSOs (J084957.97+510829.0 and J111023.85+032136.1) the S/N in the SDSS spectra does not allow us to place stringent constraint on the rest equivalent width of Ca II absorption. In the case of J082153.82+503120.4 the limiting rest equivalent width is good enough to rule out strong Ca II absorption. In Fig. 18 we plot the rest equivalent width of Ca K line against the integrated 21-cm optical depth for all the quasar sight lines (Tables 2 and 5). In the QGPs whenever there is 21-cm absorption detection it is also accompanied by the detection of Ca II absorption with rest equivalent width greater than 0.3 \AA . However, the presence of strong Ca II absorption alone does not guarantee the detection of 21-cm absorption as we found in the case of sight lines towards J122847.42+370612.0 (Table 2) and Q0446-208 (Table 5).

The rest equivalent widths of Ca II are available for

² It should be noted that the upper limit of $W_r(\text{Ca II } \lambda 3935) > 1.07 \text{ \AA}$ in this case is significantly higher than the values of $W_r(\text{Ca II } \lambda 3935)$ in the case of other QGPs and DLAs with 21-cm detections (see Tables 2 and 5), and Fig. 18.

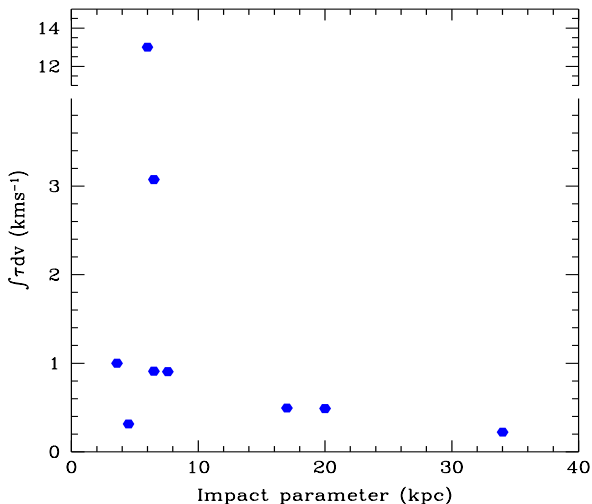


Figure 19. The integrated 21-cm optical depth is plotted against impact parameter for $z_{abs} \lesssim 1$ DLAs with 21-cm detections from Table 4 of Rao et al. (2003).

7 DLAs at $z \leq 1.0$ that are searched for 21-cm absorption (Rao et al. 2003; Kanekar & Chengalur 2003; Nestor et al. 2008; Zych et al. 2009). Interestingly only one of them has Ca II equivalent width greater than 0.3 \AA . This is very much different from the 21-cm detection in the case of QGPs. There are a few interesting differences to note. First of all, the typical impact parameters of the DLAs used in Fig. 19 are less than 10 kpc while for the QGPs values are typically between 10 kpc to 20 kpc. The 21-cm optical depth, measured in QGPs is typically less than what one measures in the case of DLAs. The low Ca II equivalent width measured in the case of DLAs, despite having higher 21-cm optical depth and smaller impact parameters may be related to the low metallicity of the high- z gas. Indeed Nestor et al. (2008) find that only 25% of the DLAs known at $0.6 \leq z_{abs} \leq 1.3$ have $W(\text{Ca II}) \geq 0.35 \text{ \AA}$. Thus DLAs may be a biased population that avoids sight lines through dusty star-forming galaxies.

4.4 Implications for high- z 21-cm surveys

Detectability of 21-cm absorption depends on $N(\text{H I})$, T_s and the fraction of the background source covered by the absorbing gas. As described before, most of the 21-cm absorption surveys have been designed to detect 21-cm absorption from gas pre-selected by the presence of a DLA or strong Mg II absorption (e.g. Briggs & Wolfe, 1983; Carilli et al. 1996; Lane 2000; Kanekar & Chengalur 2003, 2009a; Curran et al. 2007; Gupta et al. 2007, 2009; Srianand et al. 2010). In the case of DLAs, there is a possible decline in the 21-cm detection rate with increasing redshift (Kanekar & Chengalur 2003). Since for the DLAs the total $N(\text{H I})$ along the line of sight is known from the damped Lyman- α line, the decline in 21-cm absorption detection rate could be related either to the redshift evolution of spin temperature of the gas or to the redshift evolution of the covering factor (Kanekar & Chengalur 2003; Curran & Webb 2006; Kanekar et al. 2009b). However these results are based on a

small number of systems and in addition at $z \lesssim 2$ the DLA samples to search for 21-cm absorption are poorly defined.

Most of the successful searches for 21-cm absorption are based on Mg II pre-selection. A systematic survey of 21-cm absorption at $1.10 \leq z \leq 1.45$ using ~ 400 hrs of GMRT time has resulted in the largest number of 21-cm detections till now (Gupta et al. 2007, 2009). This, together with a shallower survey at $z \lesssim 1$ by Lane (2000), suggests a possible decline in the 21-cm absorber number density (n_{21}) with increasing z . This is in contrast to a strong increase in the Mg II number density over the same redshift range (see Fig. 11 of Gupta et al. 2009).

Results presented here suggest that, while the detection rate of 21-cm absorption from QGPs is 50% when the impact parameter is less than ~ 20 kpc, nearly in every case of non-detection the quasar sight line does not pass through either the stellar disk or the extended H I gas. Semi-analytical model of galaxy evolution and direct observations from GOOD and GEMS fields suggest a decrease in the optical size of the galaxies from $z \sim 0$ to $z \sim 2$ (Mo et al. 1998, Ravindranath et al. 2004; Trujillo et al. 2006). The observations are consistent with the size of a galaxy at a given stellar mass at $z \sim 1.3$ to be $\sim 70\%$ that of a galaxy at $z \sim 0$. Semi-analytic models coupled with Millennium dark matter simulations suggests that the radius of the H I gas at $z \sim 1$ is roughly half of that at $z \sim 0$ (Obreschkow & Rawlings, 2009). Based on this we expect the impact parameter around a typical galaxy at $z \sim 1.3$ to be a factor 1.5 to 2 less than the value of ~ 20 kpc we find for the QGPs and $z \lesssim 1$ DLAs (Rao et al. 2003). Therefore, the observed decrease in n_{21} could be a consequence of the small size of the optical disk and the extent of associated cold H I disk/halo. This needs to be understood in the context of the observed increase in the number density of absorption systems with redshift at optical/UV wavelengths. Obviously, this requires identifying both (1) the physical processes that determine the absorption cross-section and (2) the underlying population of absorbing galaxies. The SDSS database provides the means to make progress in this direction for 21-cm absorbers by constructing systematic samples of QGPs and RGP.

Spectral stacking methods have shown that high equivalent width Mg II systems are possibly associated with star forming regions (Noterdaeme, Srianand & Mohan, 2010; Ménard et al. 2009). It is also found that the average emission line flux for a given equivalent width range depends only weakly on the redshift (Ménard et al. 2009). All this suggests that stacked spectra of Mg II systems with 21-cm absorption should show stronger emission lines than the ones without 21-cm absorption. It will be interesting to check this once we have a sufficient number of 21-cm absorbers.

5 SUMMARY

We have presented the results of our GMRT *mini*-survey to search for 21-cm absorption in a sample of 5 QGPs (total 9 sight lines) at $0.03 \leq z \leq 0.18$. We report one clear detection of 21-cm absorption in the quasar ($z_q = 2.626$ SDSS J124157.54+633241.6) – ($z_g = 0.1430$ SDSS J124157.26+633237.6). In this case the quasar sight line pierces through the stellar disk of the galaxy. We infer metallicity, star-formation rate and reddening for the galaxy from

the SDSS spectrum. The column density inferred from the reddening estimates are consistent with the 21-cm absorbing gas being cold.

Combining our sample with the $z \leq 0.1$ QGPs (10 additional sight lines with impact parameter less than 20 kpc) available from the literature, we show the detectability of 21-cm absorption with integrated optical depth in excess of 0.1 km/s to be $\sim 50\%$ when the impact parameter is less than ~ 20 kpc. Using the surface brightness profiles and well established relationship between the optical size and extent of the H I disk (inferred from 21-cm emission observations) known for *nearby* galaxies, we conclude that in most of the cases of 21-cm absorption non-detection, the sight lines may not be passing through the H I gas.

We also find that whenever 21-cm absorption is seen Ca II absorption is detected in the optical spectrum. However, the reverse is not true. This means even at low redshifts metal absorption may originate from a larger area where the H I gas may be warm (high T_s) or ionized. Further we notice that $z < 1$ DLAs with 21-cm absorption detections have lower Ca II equivalent widths despite having higher 21-cm optical depths and smaller impact parameters. This suggests that the current sample of DLAs may be a biased population that avoids sight lines through dusty star-forming galaxies.

At present the sample size is small and H I 21-cm emission maps are not available for most of the objects in the sample to investigate the dependence of detectability on various quantities like (i) extent of the H I disk, (ii) metallicity and star-formation rate, (iii) dependence of 21-cm absorption on the type of galaxies, and (iv) the role of environmental factors such as tidal interactions and merger effects. The SDSS database provides the means to perform a systematic study to investigate these issues and understand the nature of 21-cm absorbers.

6 ACKNOWLEDGEMENTS

We thank the referee, Vivienne Wild, for the very useful and detailed comments. We wish to thank Vijay Mohan and Swara Ravindranath for useful discussions. We thank GMRT staff for their co-operation during the observations. GMRT is run by the National Centre for Radio Astrophysics of the Tata Institute of Fundamental Research. Galaxy spectra obtained at the Apache Point Observatory were made using the 3.5-meter telescope, which is owned and operated by the Astrophysical Research Consortium. We acknowledge the use of SDSS spectra from the archive at <http://www.sdss.org/>. Funding for the SDSS and SDSS-II has been provided by the Alfred P. Sloan Foundation, the Participating Institutions, the National Science Foundation, the U.S. Department of Energy, the National Aeronautics and Space Administration, the Japanese Monbukagakusho, the Max Planck Society, and the Higher Education Funding Council for England. D.V.B is funded through NASA LTSA grant NNG05GE26G.

REFERENCES

Argence, B., Lamareille, F., 2009, *A&A*, 495, 759
 Arp, H., Sargent, W.L.W., Willis, A.G., Oosterbaan, C.E., 1979, *ApJ*, 230, 68

Boisse, P., Dickey, J.M., Kazes, I., Bergeron, J., 1988, *A&A*, 191, 193
 Bechtold J., Ellingson E., 1992, *ApJ*, 396, 20
 Bergeron J., Boissé P., 1991, *A&A*, 243, 344
 Borthakur S., Tripp T.M., Yun M.S., Momjian E., Meiring J.D., Bowen D.V., York D.G., 2010, *ApJ*, 713, 131
 Bosma A., 1981, *AJ*, 86, 1825
 Bowen, D.V., Pettini M., Penston M.V., Blades C., 1991, *MNRAS*, 249, 145
 Broeils A.H., Rhee M.-H., 1997, *A&A*, 324, 877
 Briggs F.H., Wolfe A.M., 1983, *ApJ*, 268, 76
 Carilli, C.L., van Gorkom, J.H., 1992, *ApJ*, 399, 373
 Carilli C.L., Lane W., de Bruyn A.G., Braun R., Miley G.K., 1996, *AJ*, 111, 1830
 Catinella B., Haynes M.P., Giovanelli R., Gardner J.P., Connolly A.J., 2008, *ApJ*, 685, L13
 Churchill C.W., Kacprzak G.G., Steidel C.C., 2005, *astro-ph/0504392*
 Corbelli, E.S., Schneider, S.E., 1990, *ApJ*, 356, 14
 Curran S.J., Webb J.K., 2006, *MNRAS*, 371, 356
 Curran S.J., Tzanavaris P., Murphy M.T., Webb J.K., Pihlstrom Y.M., 2007, *MNRAS*, 381, L6
 de Blok, W.J.G., Walter F., Brinks E., Trachternach C., Oh S.-H., Kennicutt R.C., 2008, *AJ*, 136, 2648
 Fisher J.R., Tully R.B., 1981, *ApJS*, 47, 139
 Gordon K.D., Clayton G.C., Misselt K.A., Landolt A.U., Wolff M.J., 2003, *ApJ*, 594, 279
 Greisen E.W., Spekkens K., van Moorsel G.A., 2009, *AJ*, 137, 4718
 Gupta N., Srianand R., Petitjean P., Khare P., Saikia D.J., York D.G., 2007, *ApJ*, 654, L111
 Gupta N., Srianand R., Petitjean P., Noterdaeme P., Saikia D.J., 2009, *MNRAS*, 398, 201
 Haynes M.P., Giovanelli R., Roberts M.S., 1979, *ApJ*, 229, 83
 Haschick, A.D., Burke, B.F., 1975, *ApJ*, 200, L137
 Haschick, A.D., Crane, P.C., Greenfield, P.E., Burke, B.F., Baan, W.A., 1980, *ApJ*, 239, 774
 Haschick, A.D., Crane, P.C., Baan, W.A., 1983, *ApJ*, 269, L43
 Hwang, C., Chiou, S., 2004, *ApJ*, 600, 52
 Kacprzak, G.G., Churchill C.W., Steidel C.C., Murphy M.T., 2008, *AJ*, 135, 922
 Kanekar N., Chengalur J.N., 2003, *A&A*, 399, 857
 Kanekar N., Prochaska J.X., Ellison S.L., Chengalur J.N., 2009a, *MNRAS*, 396, 385
 Kanekar N., Lane W.M., Momjian E., Briggs F.H., Chengalur J.N., 2009b, *MNRAS*, 394, L61
 Lah P. et al., 2009, *MNRAS*, 399, 1447
 Lane W., 2000, PhD Thesis, University of Groningen
 Marinoni C., Monaco P., Giuricin G., Costantini B., 1999, *ApJ*, 521, 50
 Ménard B., Wild V., Nestor D., Quider A., Zibetti S., 2010, *astro-ph/0912.3263*
 Meyer M.J., Zwaan M.A., Webster R.L., Staveley-Smith L., Ryan-Weber E., Drinkwater M.J., Barnes D.G., 2004, *MNRAS*, 350, 1195
 Mo H.J., Mao S., White S.D.M., 1998, *MNRAS*, 295, 319
 Murdoch, H.S., Hunstead, R.W., Arp, H.C., Blades, J.C., Burbidge, E.M., Condon, J.J., 1983, *ApJ*, 265, 610
 Nestor D.B., Pettini M., Hewett P.C., Rao S., Wild V., 2008, *MNRAS*, 390, 1670
 Noordermeer E., van der Hulst J.M., Sancisi R., Swaters R.A., van Albada T.S., 2005, *A&A*, 442, 137
 Noterdaeme P., Ledoux C., Srianand R., Petitjean P., Lopez S., 2009, *A&A*, 503, 765
 Noterdaeme P., Srianand R., Mohan V., 2010, *MNRAS*, 403, 906
 Obreschkow D., Rawlings S., 2009, *MNRAS*, 400, 6650
 Oosterloo T., Fraternali F., Renzo S., 2007, *AJ*, 134, 1019
 Osterbrock D.E., Ferland G.J., 2006, *Astrophysics of gaseous neb-*

- ulae and active galactic nuclei, 2nd. ed., Sausalito, CA: University Science Books
- Östman L.G.A., Mörtzell E., 2006, *A&A*, 450, 971
- Pettini M., Pagel B.E.J., 2004, *MNRAS*, 348, L59
- Quashnock J.M., 2008, *AAS*, 212, 2603
- Rao, S.M., Nestor, D.B., Turnshek, D.A., Lane, W.M., Monier, E.M., Bergeron, J., 2003, *ApJ*, 595, 94
- Ravindranath S. et al., 2004, *ApJ*, 604, L9
- Rosenberg J.L., Schneider S.E., 2002, *ApJ*, 567, 247
- Schneider S.E., Corbelli E., 1993, *ApJ*, 414, 500
- Spergel D.N. et al., 2007, *ApJS*, 170, 377
- Srianand, R., Gupta, N., Petitjean, P., Noterdaeme, P., Saikia, D. J., 2008, *MNRAS*, 391, L69
- Srianand R., Gupta N., Petitjean P., Noterdaeme P., Ledoux C., 2010, *MNRAS*, in press (astro-ph/1002.4620)
- Steidel C., 1995, astro-ph/9509098
- Stickel, M., Fried, J.W., Kühr, H., 1989, *A&A*, 224, L27
- Tripp, Todd M.; Bowen, David V., astro-ph/0510312
- Trujillo I. et al., 2006, *ApJ*, 650, 18
- Verheijen M., van Gorkom J.H., Szomoru A., Dwarakanath K.S., Poggianti B.M., Schiminovich D., 2007, *ApJ*, 668, L9
- Walter F., Brinks E., de Blok W.J.G., Bigiel F., Kennicutt R.C., Thornley M.D., Leroy A., 2008, *AJ*, 136, 2563
- Wiklind, T., Combes, F., 1995, *A&A*, 299, 382
- Wild V., Hewett P.C., 2005, *MNRAS*, 361, L30
- Wild V., Hewett P.C., Pettini M., 2006, *MNRAS*, 367, 211
- Wild V., Hewett P.C., Pettini M., 2007b, *MNRAS*, 374, 292
- Wild V., Kauffmann G., Heckman T., Charlot S., Lemson G., Brinchmann J., Reichard T., Pasquali A., 2007a, *MNRAS*, 381, 543
- Womble D.S., Junkkarinen V.T., Cohen R.D., Burbidge E.M., 1990, *AJ*, 100, 1785
- Womble D.S., 1993, *PASP*, 105, 1043
- York D.G., Khare P., Vanden Berk D., Kulkarni V.P., Crotts A.P.S., Lauroesch J.T., Richards G.T., Schneider D.P. et al., 2006, *MNRAS*, 367, 945
- Zwaan M.A., Meyer M.J., Staveley-Smith L., Webster R.L., 2005, *MNRAS*, 359, L30
- Zych B.J., Murphy M.T., Hewett P.C., Prochaska J.X., 2009, *MNRAS*, 392, 1429
- Zych B.J., Murphy M.T., Pettini M., Hewett P.C., Ryan-Weber E.V., Ellison S.L., 2007, *MNRAS*, 379, 1409